JCTC Journal of Chemical Theory and Computation

ARTICLE

pubs.acs.org/JCTC

Artificial Bee Colony Optimization of Capping Potentials for Hybrid Quantum Mechanical/Molecular Mechanical Calculations

Christoph Schiffmann and Daniel Sebastiani*

Physics Department, Freie Universität Berlin, Arnimallee 14, 14195 Berlin, Germany

Supporting Information

ABSTRACT: We present an algorithmic extension of a numerical optimization scheme for analytic capping potentials for use in mixed quantum−classical (quantum mechanical/molecular mechanical, QM/MM) ab initio calculations. Our goal is to minimize bond-cleavage-induced perturbations in the electronic structure, measured by means of a suitable penalty functional. The optimization algorithm—a variant of the artificial bee colony (ABC) algorithm, which relies on swarm intelligence—couples deterministic (downhill gradient) and stochastic elements to avoid local minimum trapping. The ABC algorithm outperforms the conventional downhill gradient approach, if the penalty hypersurface exhibits wiggles that prevent a straight minimization pathway. We characterize the optimized capping potentials by computing NMR chemical shifts. This approach will increase the accuracy of QM/MM calculations of complex biomolecules.

1. INTRODUCTION

Accurate simulation of structural and dynamical phenomena of complex biomolecular systems by means of first-principles molecular dynamics simulation techniques is still a challenge for modern physics and chemistry. Despite enormous progress in recent decades, predictive modeling of the interplay of intramolecular and intermolecular interactions is still far from being a routine problem. For determination of structural data in biophysics and biochemistry, the combination of spectroscopic experiments with advanced theoretical predictions and computer simulations is becoming increasingly popular, because this combination often yields a predictive power above the sum of the individual approaches.[1−9] Nevertheless, the first-principles prediction of noncovalent packing effects and the ab initio prediction of experimentally observable spectra is not possible for regular biosystems because of their inherent complexity and, last but not least, their sheer size. Thus, one has to resort either to the modeling of elementary subunits[10−14] or alternatively to hybrid quantum-mechanical + mechanical modeling (QM/MM) approaches.[15−31] One of the difficulties of such a hybrid approach is the interface region between the two different regions. If one of the atoms is located in the quantum (QM) region and the other in the classical (MM) part, then a chemical bond is "broken" as a consequence. This situation is sketched in Figure 1. Similar problems arise when MM atoms are located near a QM region, because the QM and MM descriptions are not genuinely compatible. Thus, a suitable interface has to be used, which can mutually couple the two schemes in a realistic way.

There are several well-established methods to tackle the bond saturation problem, in particular hydrogen[32] or fluorine[33] atoms, precomputed (frozen) atomic orbitals,[34,35] generalized hybrid orbitals,[36−38] quantum capping potentials,[39−42] or designed heptavalent capping potentials.[43] Complementary, effective fragment potentials[44,45] and field-adapted adjustable density matrix assembler[46−48] approach the repartiotioning problem itself. Our approach is conceptually simpler than most of the former ones; we aim at designing a fictitious capping atom to saturate the QM subsystem, which is realized by a regular atomic pseudopotential.

Specifically, we want to improve a method that has been developed recently[49] in view of more complex bond-cleavage situations. This approach is based on analytical effective core potentials (pseudopotentials) of Goedecker−Teter−Hutter (GTH) type,[50,51] in line with previous QM/MM studies.[14,23,52] Our goal is to optimize the pseudopotential parameters in such a way that the change of electronic density in the quantum part of a QM/MM calculation is minimal with respect to a "full-QM" calculation.

In this way, we also ensure that structural parameters and spectroscopic properties in the direct neighborhood of a QM/MM bond cleavage are modeled with a high degree of reliability.

To achieve this aim, we define a penalty functional that quantifies the deviation of the electronic density in a molecular fragment from the corresponding density in the complete molecule, while simultaneously penalizing changes in the equilibrium bond distance and frequency. The penalty functional is minimized iteratively by varying the coefficients of the capping potential placed at the bond-cleavage site.

However, a straightforward mimization approach like steepest descent[53,54] or a simplex method[55] carries the risk of getting stuck in local minima. To avoid this pitfall, we aim for global optimization including stochastic elements by means of a swarm intelligence-based algorithm. In recent years, biology-inspired algorithms[56,57] turned out to be more effective than conventional algorithms.[58]

In this work, we employ a variation of the artificial bee colony algorithm[59−61] (ABC), which mimicks the foraging behavior of honeybees for function minimization. We are especially interested in proving the usablility for optimizations within electronic structure calculations and studying the performance of the algorithm. The optimized capping potentials are intended to

Received: December 10, 2010
Published: April 07, 2011

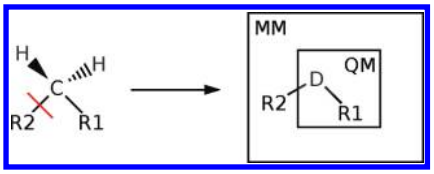

Figure 1. General QM/MM repartioning principle in which the C−R2 bond crosses the QM/MM border and is cleaved. The CH_2 group is replaced by a capping potential associated with a fictitious particle D, saturating the C−R1 bond and hence terminating the QM region.

saturate the quantum region in hybrid QM/MM calculations. In most cases, this saturation affects a single C−C bond and can therefore be done by means of a hydrogenoid atom; however, the properties of this hydrogenoid atom should resemble as much as possible the characteristics of the carbon atom that has been "cut" out from the quantum calculation. Hence, we need a fictitious atom that is monovalent but behaves like a (four-valent) carbon atom in terms of bond distance, potential energy curve(s), and electronic structure.

We further characterize the perturbative effect of bond cleavage by means of NMR chemical shifts, which are known to be particularly sensitive to both intramolecular electronic structure and intermolecular effects such as hydrogen bonding.[62−66] Hence, we can not only gauge the direct perturbing effect of the cleaved bond on the electronic structure of the remaining part of a molecule but also quantitatively describe how strongly its response properties are tainted by the QM/MM bond cleavage.

2. OPTIMIZATION APPROACH

In QM/MM calculations, the dummy atom has to saturate the last covalent bond in the quantum region of the molecule, that is, the bond that is cleaved by QM/MM repartitioning. The true character of the bond, however, cannot be easily reproduced by a simple terminal atom. It is therefore necessary to tune the dummy's properties in a way that the resulting deviation in the quantum region's electronic structure is minimal. To do so, one has to find a capping potential that equips the dummy with the desired properties.

2.1. Definition of Penalty Functional. Our optimization scheme aims to find a capping potential V_{cap} that gives rise to an electronic density in the quantum region ($\rho[V_{cap}]$) that deviates only in a minimal manner from the reference electron density (ρ^{ref}), that is, the density when the whole molecule is quantum-mechanically treated. Further, we want to preserve the equilibrium bond length and vibrational properties of the bond that is cleaved to allow for an easy coupling of the first classical MM atom and to avoid the need for additional geometric constraints (see Komin and Sebastiani[49] and von Lilienfeld-Toal et al.[67] for a more detailed description).

Therefore, we define a functional that penalizes deviations of these properties from their target values obtained in a full-QM calculation:

$$\mathscr{P}[V_{cap}] = \omega_\rho \sum_{j=1}^{N_{geo}} \int_\Omega d^3r \, |\rho_j^{ref}(\mathbf{r}) - \rho_j[V_{cap}](\mathbf{r})|^2 + \omega_f \sum_{j=1}^{N_{geo}} |\mathbf{F}_j^{ref} - \mathbf{F}_j[V_{cap}]|^2 + \omega_e \sum_{j=2}^{N_{geo}} |(E_j^{ref} - E_1^{ref}) - (E_j[V_{cap}] - E_1[V_{cap}])|^2 \quad (1)$$

The integration volume Ω is restricted to an area where penalization is meaningful, that is, the union of spheres around all QM atoms except the dummy with radii r_{cov}^{spc}, where r_{cov}^{spc} is the covalent radius of the atom species (spc). $\mathbf{F}$ denotes the force acting on the dummy (with respect to its uncapped counterpart) and E is the total energy. ω_ρ, ω_f, and ω_e are weighting factors that ensure an adequate relative importance between density, force, and energy penalization. Finally, the penalty is evaluated for $N_{geo} = 3$ molecular geometries, which correspond to variations of the cleaving bond length.

We note at this point that we have replaced a multielectron group (e.g., methyl) with a fictitious monovalent atom, which changes the total number of electrons in the system. Hence, the integration of a direct density difference can never vanish completely, unless the affected regions are entirely excluded from the integration. This also leads to the effect that the penalty functional will in general never reach zero during a capping potential optimization.

2.2. GTH Pseudopotentials. We assume that an optimal capping potential can be expressed as an analytical GTH potential:[50,51]

$$V_{cap}(\mathbf{r},\mathbf{r}') = V_{loc}(\mathbf{r}) + \sum_{l=0}^{l_{max}} V_l(\mathbf{r},\mathbf{r}') \quad (2)$$

consisting of a local component V_{loc}, eq 3, and 0−3 (l_{max}) nonlocal components V_l, eq 4, with the form

$$V_{loc}(\mathbf{r}) = \frac{-Z_{ion}}{r} \operatorname{erf}\left(\frac{r}{\sqrt{2}r_{loc}}\right) + \exp\left[-\frac{1}{2}\left(\frac{r}{r_{loc}}\right)^2\right] \sum_{j=1}^{4} C_j \left(\frac{r}{r_{loc}}\right)^{2(j-1)} \quad (3)$$

$$V_l(\mathbf{r},\mathbf{r}') = \sum_{i=1}^{3}\sum_{j=1}^{3}\sum_{m=-l}^{+l} Y_{l,m}\left(\frac{\mathbf{r}}{r}\right) p_i^l(r) h_{i,j}^l p_j^l(r') Y_{l,m}\left(\frac{\mathbf{r}'}{r'}\right) \quad (4)$$

$$p_i^l(r) = \frac{\sqrt{2} r^{l+2(i-1)} \exp\left(-\frac{r^2}{2r_l^2}\right)}{r_l^{l+(4i-1)/2} \sqrt{\Gamma\left(l+\frac{4i-1}{2}\right)}} \quad (5)$$

Z_{ion} is a valence charge, $Y_{l,m}$ are spherical harmonics, and $h_{i,j}^l$ are scalars that define the energetic weighting of projectors $p_{i/j}^l$, eq 5, in each angular momentum channel l.

A potential of this type is fully defined via the set of N_σ parameters:

$$\{r_{loc}, C_1, C_2, C_3, C_4, r_0, h_{1,1}^0, h_{2,2}^0, h_{3,3}^0, r_1, h_{1,1}^1, \ldots, r_2, h_{1,1}^2, \ldots\} \quad (6)$$

In the following, we use $\{\sigma\}$ as simplified notation for this set.

From physical considerations, we impose an allowed interval for each parameter. Thus, the optimization takes place in an N_σ dimensional orthorhombic manifold in $\mathbb{R}^{N_\sigma}$.

2.3. Artificial Bee Colony (ABC). The actual optimization algorithm is taken from the field of swarm intelligence and as such is inspired by nature itself. It mimicks the foraging behavior of honeybees to sample a scalar function defined on an N_σ-dimensional unit cube (U_σ) in an efficient manner. We use a set of linear transformations to rescale and shift the allowed parameter space into the unit cube.

We define a *population* as a set of N_{pop} *agents*, each representing a configuration $\{\sigma\}_a \in U_\sigma$ and the corresponding penalty

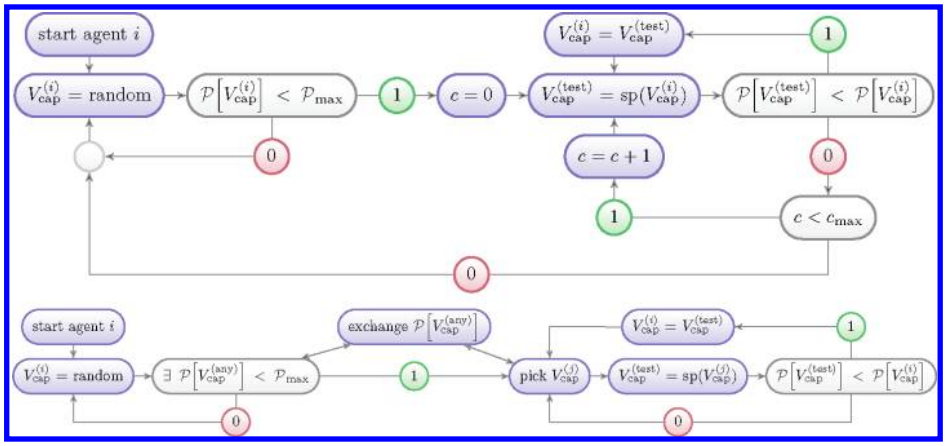

Figure 2. Employee-type (top) and onlooker-type (bottom) agents.

$\mathscr{P}[\{\sigma\}_a]$. This artificial bee colony (ABC) algorithm distiguishes three types of agents which, like honeybees in nature, fulfill simple but different tasks:

- Scout-type agents have the biggest exploration tendency of the three types. A scout chooses in every cycle a random point $\{\sigma\}$ from uniform distribution in U_σ and moves unconditionally to that spot (global sampling).
- Employee-type agents have an additional local sampling component. An employee type starts like a scout but examines in each cycle a random spot $\{\sigma\}'$ from a uniform distribution in a sphere of radius r_s around its present position $\{\sigma\}$. The agent moves only if $\mathscr{P}[\{\sigma\}'] < \mathscr{P}[\{\sigma\}]$. Furthermore, if the agent cannot move for N_a successive cycles, it *abandons* its present position and restarts the search again from a fully random spot in U_σ.
- Onlooker-type agents act, from the point of view of the entire agent population, as feedback and amplify the exploitation of promising areas in U_σ that have been found by other agents. Equipped with knowledge of all agents' positions and penalties, an onlooker type randomly choses another agent's parameter set $\{\sigma\}$, inversely weighted by the penalties. Then it chooses a spot $\{\sigma\}'$ from a uniform distribution in a sphere of radius r_s around $\{\sigma\}$ and moves if $\mathscr{P}[\{\sigma\}']$ is smaller than its original penalty. Thus, this type depends on the other agents' results and ensures that good parameter regions are not lost during an employee-type resetting.

A more detailed description of employee- and onlooker-type agents and their "interactions" is given in the flowcharts in Figure 2.

Optimization starts with *initialization* of the population. In this phase, every agent, regardless of its type, is randomly placed in U_σ. Afterward, the ABC algorithm performs N_{cycle} *cycles*, each a sequence of three steps:

1. Send the employee- and onlooker-type agents to their destinations and evaluate the penalties.
2. Place the scout-type agents and the employee-type agents that abandoned their positions randomly in U_σ.
3. Store the pseudopotential parameter set $\{\sigma\}$ with the lowest penalty in the present population.

Thus, the interaction of the three types of agents, determined by the ABC algorithm, successivly searches for the global minimum $\mathscr{P}[\{\sigma\}_{min}]$ of the penalty functional.

The pseudocode of the ABC algorithm is given in Chart 1.

2.4. Evolution and Convergence of Optimization. We define a combined index for the evolution of all agents:

$$\tau := i \cdot N_{pop} \tag{7}$$

where $0 \le i \le N_{cycle}$ denotes the current optimization cycle. Thus, τ corresponds to the computational cost under the assumption that determination of the penalty $\mathscr{P}[\{\sigma\}]$ has a fixed computational cost for all choices of $\{\sigma\}$. As this assumption cannot be enforced formally, we limit the number of self-consistent-field (SCF) iterations during the wave function optimization for each penalty evaluation to 30. With this combined index we can describe the evolution of the ensemble of agents during one optimization run via

$$\begin{aligned} \mathscr{P}(\tau = 0) &:= \min_{j=1,\ldots,N_{pop}} \{\mathscr{P}[\{\sigma\}_{j,i=0}]\} \\ \mathscr{P}(\tau > 0) &:= \min\left(\mathscr{P}(\tau - N_{pop}), \min_{j=1,\ldots,N_{pop}} \{\mathscr{P}[\{\sigma\}_{j,i\neq 0}]\}\right) \end{aligned} \tag{8}$$

where $\{\sigma\}_{j,i}$ are the pseudopotential parameters of agent j in the ith optmization cycle (the case $i = 0$ denotes the initialization phase). Hence, (τ) and $\{\sigma\}(\tau)$ refer to the minimal penalty after an optimization time τ and the corresponding pseudopotential parameter set.

To account for the stochastic nature of the optimization process, we run N_{trial} independent optimizations for each set of control parameters (i.e., the number of employee- and onlooker-type agents as well as the radius of the neighborhood sphere r_s). This enables us to describe the convergence behavior in statistical terms. We distinguish between different optimization runs by a new superscript $1 \le k \le N_{trial}$:

$$\mathscr{P}_{min}(\tau) = \min_{k=1,\ldots,N_{trial}} \{\mathscr{P}^k(\tau)\} \tag{9}$$

$$\mathscr{P}_{max}(\tau) = \max_{k=1,\ldots,N_{trial}} \{\mathscr{P}^k(\tau)\} \tag{10}$$

Equations 9 and 10 describe a window in which all $\mathscr{P}^k(\tau)$ are located for a fixed setting of control parameters (best- and worst-case scenarios).

2.5. Computational Details. We perform all calculations within density functional theory[68−70] using the BLYP[71,72] exchange−correlation functional, as implemented in the CPMD package.[73,74]

Chart 1. Pseudocode of the ABC Algorithm

```
initialize population randomly
for i = 1...N_cycles do
        run employee types
        run onlooker types
        run scout types
        abandon solutions
        update best solution
done
```

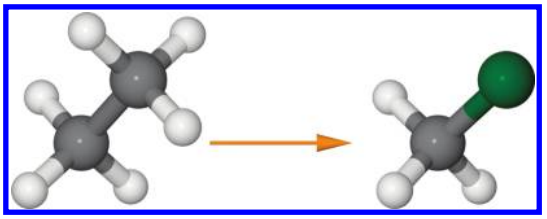

Figure 3. Ethane (C_2H_6) as test system for benchmarking. One methyl group is replaced by a capping potential (green particle), which saturates the remaining methyl group.

We use standard norm-conserving pseudopotentials[50,51] and an energy cutoff of 70 Ry for the plane-wave expansion of the Kohn−Sham orbitals.

Calculation of spectroscopic parameters, for example, NMR chemical shifts, is done within density functional perturbation theory as implemented in the linear response package of CPMD.[75−77]

3. RESULTS

3.1. Stochastic Optimization of Capping Potentials. We have applied the ABC algorithm to the optimization of GTH-type capping potentials V_{cap} for hybrid QM/MM calculations within DFT. In particular, we have examined the influence of control parameters of the ABC algorithm (i.e., the number of employee and onlooker type agents and the radius of the neighborhood sphere r_s) on the optimization process. For this purpose, we benchmarked a series of capping potential optimizations for an isolated ethane molecule (C_2H_6) in which one methyl group is replaced by a capping potential, with respect to a dummy particle D, as shown in Figure 3.

We begin the presentation of our optimization benchmarks with the effect of number of employee- (E) and onlooker- (O) type agents on evolution of the ensemble of agents for different population sizes. For the initial benchmarks, a fixed value of $r_s = 0.2$ is used. N_a is set to 10 and the penalty weights are $\omega_\rho = 1$, $\omega_f = 0.01$, and $\omega_e = 2$ (arbitrary units). We initialize the first agent in each optimization run with the standard carbon GTH pseudopotential. To allow for a higher level of flexibility of the capping potential, we add an angular momentum channel ($l = 1$) with one projector, which leads to a 7-dimensional parameter space.

Figures 4−6 show penalty minimization over an optimization time $0 \le \tau \le 800$ for $N_{pop} = 4$, 12, and 20, respectively. Each figure shows the penalty evolution window as described by eqs 9 and 10 for different population setups $E + O = N_{pop}$. The number of trial runs is $N_{trial} = 5$ for each choice of E/O. An employee-type agent abandons its position after $N_a = 10$ unsuccessful cycles.

We observe in Figure 4 ($N_{pop} = 4$) a fast decrease of the lower penalty boundary $\mathscr{P}_{min}(\tau)$ during $\tau \le 100$ for all E/O combinations.

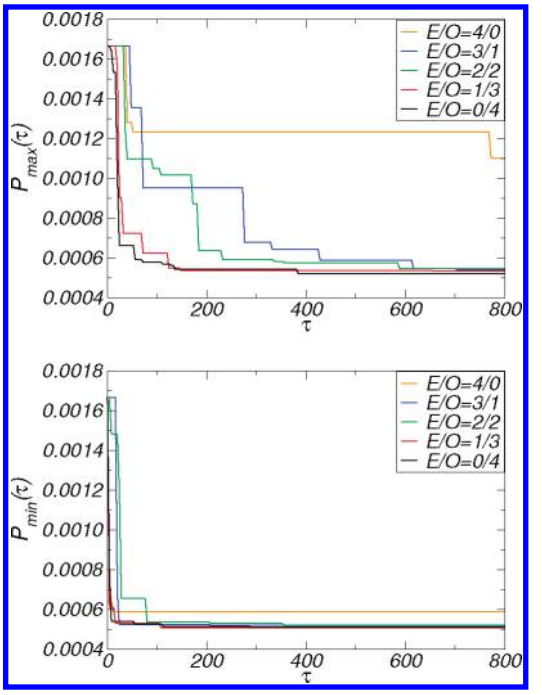

Figure 4. Population size/setup benchmarks: upper penalty boundary $\mathscr{P}_{max}(\tau)$ and lower penalty boundary $\mathscr{P}_{min}(\tau)$ with $E + O = 4$, $r_s = 0.2$, and $N_{trial} = 5$.

This boundary remains practically unchanged for the remaining optimization. On the other hand, the upper penalty boundary $\mathscr{P}_{max}(\tau)$ shows a decay comparable to that of the lower penalty boundary but only for combinations with no or few employee-type agents. For equal numbers of employee/onlooker-type agents or a higher amount of employee types, the upper penalty boundary decreases on a much slower time scale with practically no convergence in the all-employee-type case ($E = N_{pop}$).

Very similar behavior of the lower penalty boundary is observed for $N_{pop} = 12$ (Figure 5). The decrease of the upper penalty boundary is similar for combinations from 0 to 6 employee-type agents, and significantly slower for higher numbers of E. The decrease of $\mathscr{P}_{max}(\tau)$ happens on a slightly longer time scale compared to the optimization benchmarks with $N_{pop} = 4$.

This trend remains valid for $N_{pop} = 20$ (Figure 6). The decrease of the penalty window (i.e., the interval $[\mathscr{P}_{min}(\tau),\mathscr{P}_{max}(\tau)]$) is significantly slower compared to smaller populations.

As an extreme case of employee/onlooker combinations, we show in Figure 7 the upper and lower penalty boundaries for a series of $N_{trial} = 5$ optimization runs with a population consisting of only one agent of employee type and $N_a > N_{cycle}$ The lower penalty boundary reaches its minimum after an optimization time of $\tau \approx 230$. The upper penalty boundary needs nearly $\tau \approx 800$ to approach the value of the lower boundary.

The second control parameter of the optimization algorithm is the size of the neighborhood sphere r_s. Again, we run a series of independent optimizations with a fixed population setup of 3 employee and 9 onlooker types, with $N_a = 10$, $\omega_\sigma = 1$, $\omega_f = 0.01$, and $\omega_e = 2$. We show in Figure 8 the upper penalty boundary $\mathscr{P}_{max}(\tau)$ and lower penalty boundary $\mathscr{P}_{min}(\tau)$ for different radii r_s, with $N_{trial} = 5$ runs each.

We observe a steady (but slow) minimization behavior for small radii $r_s \le 0.01$. Intermediate radii ($r_s = 0.1$ and 0.2) lead to a fast decrease of the penalty window ($[\mathscr{P}_{min}(\tau),\mathscr{P}_{max}(\tau)]$).

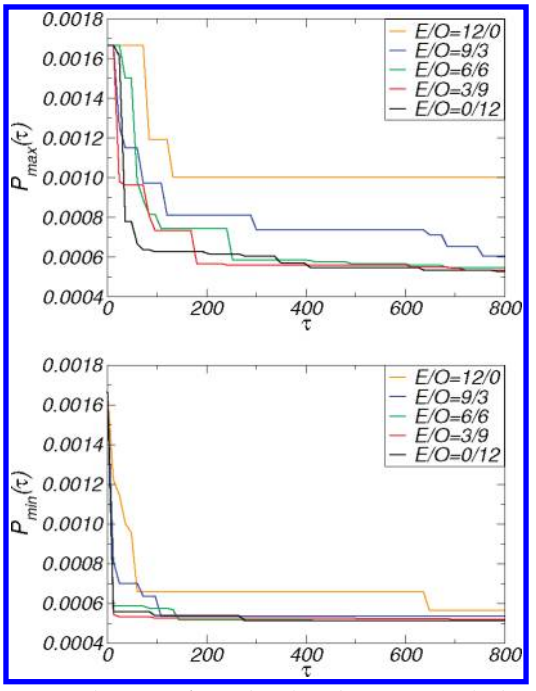

Figure 5. Population size/setup benchmarks: upper penalty boundary $\mathscr{P}_{max}(\tau)$ and lower penalty boundary $\mathscr{P}_{min}(\tau)$ with $E + O = 12$, $r_s = 0.2$, and $N_{trial} = 5$.

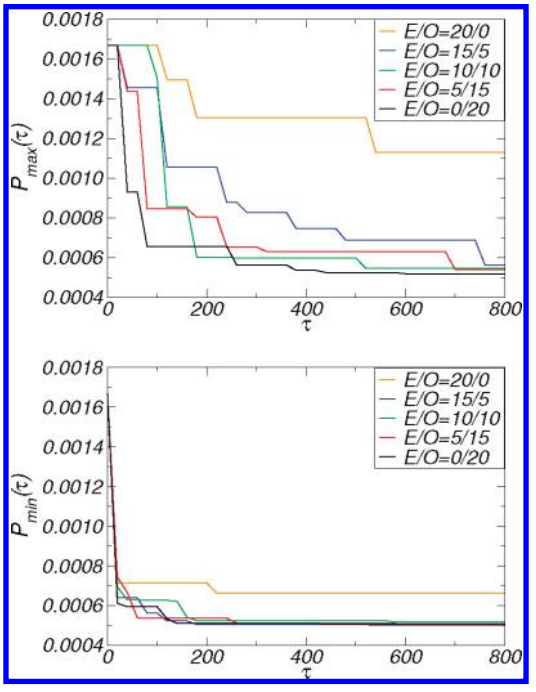

Figure 6. Population size/setup benchmarks: upper penalty boundary $\mathscr{P}_{max}(\tau)$ and lower penalty boundary $\mathscr{P}_{min}(\tau)$ with $E + O = 20$, $r_s = 0.2$, and $N_{trial} = 5$.

Bigger radii lead to a comparable decrease in the lower penalty boundary. The upper penalty boundary, however, decreases quite slowly and unsteadily.

The optimizations presented so far have all used the conventional carbon GTH pseudopotential as starting point. While this appears adequate for the particular situation of homolytic C−C

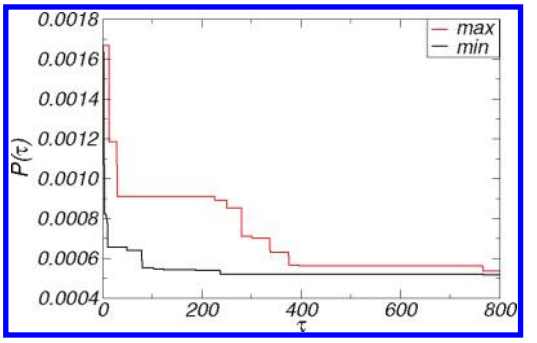

Figure 7. Single employee-type agent: lower penalty boundary $\mathscr{P}_{min}(\tau)$ and upper penalty boundary $\mathscr{P}_{max}(\tau)$ with $E = N_{pop} = 1$, $r_s = 0.2$, and $N_{trial} = 5$.

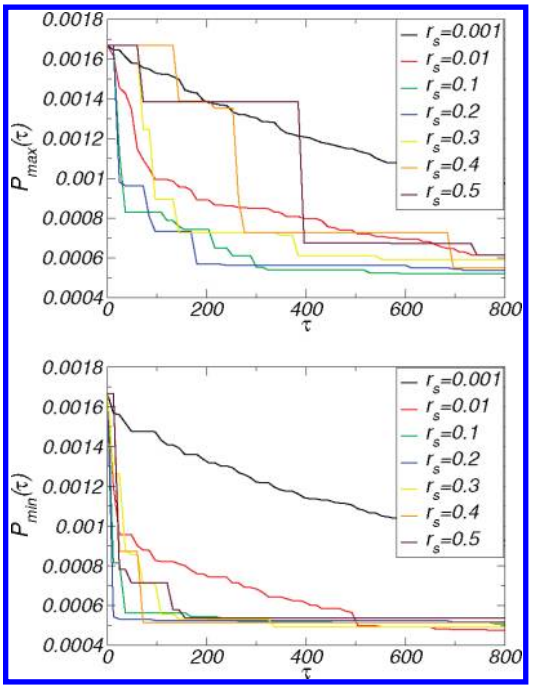

Figure 8. Sphere radius r_s benchmarks: upper penalty boundary $\mathscr{P}_{max}(\tau)$ and lower penalty boundary $\mathscr{P}_{min}(\tau)$ with $N_{pop} = 12$, $E/O = 3/9$, and $N_{trial} = 5$.

bond capping, we aim at designing capping potentials for more complex settings. In order to test the performance of our ABC algorithm in more difficult circumstances, we repeat the optimization of our C−C capping potential from a starting point with randomized capping parameters.

For a population of $E + O = 12$, $N_a = 10$, $r_s = 0.2$, $\omega_\rho = 1$, $\omega_f = 0.01$, and $\omega_e = 2$, we perform $N_{trial} = 5$ independent optimizations with varying combinations for E/O. The evolution for this unfavorable initialization of agents is shown in Figure 9.

The behavior of the lower penalty boundary is nearly identical for small to intermediate numbers of employee types. It decreases more slowly for a higher amount of employee types. The upper penalty boundary shows a similar pattern for all E/O combinations, but an equal amount of employee and onlooker types shows the best performance in an early stage of the optimization.

Regarding the combination of employee and onlooker agents, it turns out that the optimal ratio depends strongly on whether the present set of agents is "in direct view" of the final minimum,

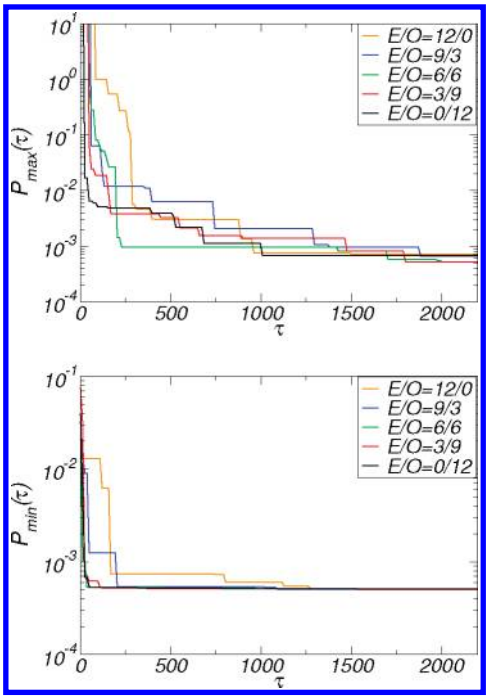

Figure 9. Population setup benchmarks: upper penalty boundary $\mathscr{P}_{max}(\tau)$ and lower penalty boundary $\mathscr{P}_{min}(\tau)$ with $E + O = 12$, $r_s = 0.2$, and $N_{trial} = 5$ with fully random initialization.

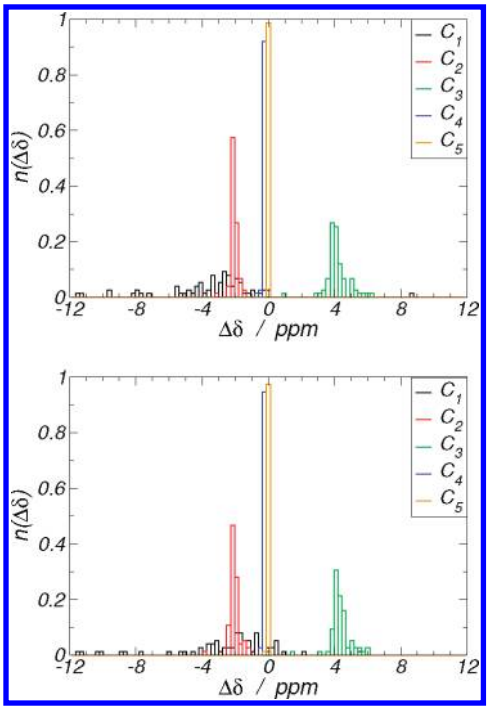

Figure 10. Distribution $n(\Delta\delta)$ of the isotropic NMR chemical shift $\Delta\delta$ of carbon atoms in hexane with V_{cap} bound to C_1 for an ensemble of 75 capping potentials obtained from independent optimizations: (top) hexane geometry; (bottom) optimized geometry for V_{cap}.

that is, in its proximity and without additional barriers on the way. For a good starting point of the optimization, for example, the feedback process inherent to onlooker agents leads to a speedup of the optimization, and zero agents of employee type are best. On the other hand, a nonoptimal starting point (as obtained via the randomized initialization) requires a certain number of agents with explorative character, that is, employee (or scout) type agents. Hence, it might eventually be useful to switch the distribution of employee versus onlooker types during the progress of the optimization. Investigation of this effect, however, exceeds the scope of the present paper.

As for the sphere radius r_s, we find that a small value leads to a slow "speed" of the agents in parameter space. A large value, on the other hand, allows for large moves. However, the plateaus in the evolution of $\mathscr{P}_{max}$ (Figure 8) for $r_s \geq 0.4$ illustrate that a large neigborhood area leads to a high rejection rate for the proposed moves of the agents. We find that an intermediate choice of $0.1 \leq r_s \leq 0.2$ leads to the fastest decay of the penalty window, due to a trade-off between the "speed" of the agents in parameter space and their rejection rate. We believe that this behavior indicates a rich structure of the penalty surface, even for this simple case of homolytic C−C bond capping.

3.2. Initial Benchmark of Optimized Capping Potentials. To examine the quality of optimized capping potentials obtained during our benchmarks, we compute electronic linear response properties for a linear alkane molecule (hexane) in which the terminal methyl group is replaced by a capping potential. In particular, we compute spectroscopic properties that involve both the occupied and excited manifold of electronic orbitals. These parameters measure the performance of our capping potential beyond the scope that is accessible by the penalty functional (eq 1) because the latter is based only on the ground-state density.

We have chosen ^{13}C NMR chemical shifts δ for the characterization of our capping potentials. These chemical shifts are the result of a complex interplay of occupied and excited electronic states. Nevertheless, they are relatively short-sighted, which means that a perturbation in the electronic spectrum reaches no further than a few covalent bonds. Hence, they allow us to monitor the range in which the QM/MM-induced bond cleavage perturbs the electronic subsystem.

Specifically, we compute the distribution of deviations of the trace of the nuclear shielding tensor $\sigma_{\alpha\beta}$ for a capped molecule with respect to a full calculation:

$$\Delta\delta = \mathrm{Tr}(\sigma_{\alpha\beta}[\text{full-QM}] - \sigma_{\alpha\beta}[\text{QM/MM}]) \qquad (11)$$

This is done (1) in the optimized geometry of the full hexane molecule and (2) in a geometry that has been optimized by use of V_{cap}. In both cases, we obtain an ensemble of chemical shift values from the ensemble of independent optimization runs.

Figure 10 shows the distribution of $\Delta\delta$ of carbon atoms C_i, where C_1 is the direct neighbor of V_{cap}. For both geometries, we observe a similar picture: $\Delta\delta$ of the direct neighbor of V_{cap} has a broad distribution with a clustering between −3 and −2 ppm. The distribution for next two carbon atoms (C_2 and C_3) have distinct peaks at −2 and 4 ppm, respectively. As for the last two carbons, we find only minor deviations, far below 1 ppm, from the reference NMR signature.

3.3. Application to Octane. While the main focus in this article is on the algorithmic performance of the ABC algorithm in the QM/MM context, we have nevertheless applied the ABC/capping potential algorithm to C−C bond cleavage in a larger molecule, specifically octane. Here, a butane fragment has been replaced by a capping potential; see Figure 11.

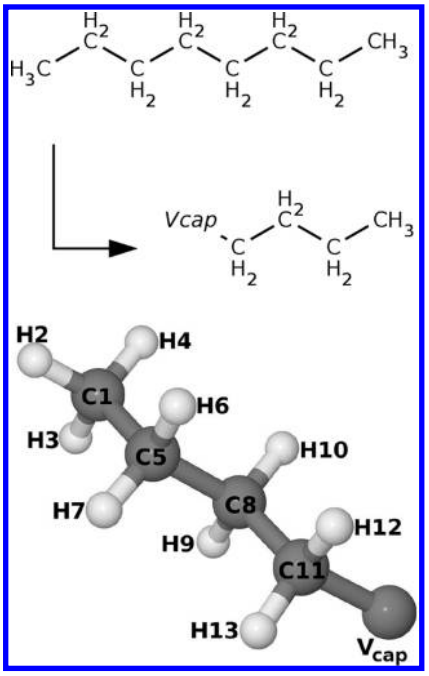

Figure 11. Reference system octane and its capped counterpart: (top) bond-capping scheme and (bottom) atom numbering.

Table 1. GTH Parameters for Regular Carbon and Optimized C−C Capping Potential V_{cap}

	r_{loc}	C_1	C_2	r_0	$h^0_{1,1}$	r_1	$h^1_{1,1}$
regular C	0.3376	−9.1285	1.4251	0.3025	9.6507		
V_{cap}	0.2101	−13.1925	3.4867	0.2416	6.2451	0.3125	9.7340
ref 49	0.7221	9.9086	−2.5466	0.5120	−3.5081	1.4664	0.2316

The optimization is performed over 500 cycles with $E = 4$ and $O = 6$, a neigborhood sphere radius of $r_s = 0.1$, and an integration volume for the density difference consisting of spheres of size 1.5× covalent radius around each atom except V_{cap}. The penalty weighting factors are $\omega_\rho = \omega_f = \omega_e = 1$. See Table 1 for the initial guess (regular carbon) and optimized capping potential parameters (V_{cap}).

All geometric parameters (shown in Table 2) of the capped octane molecule are in excellent agreement with the full octane reference. This agreement holds for our new optimized potential as well as for a previous version,[49] and to some degree even for the simpler hydrogen and fluorine cappings. While the hydrogen termination looks like an accurate way of capping when the H−C bond distance is ignored, it has a strong effect on the properties of the subsequent C−C bond. This is shown in the potential energy curve (Figure 12) of the C_8-C_{11} bond: when hydrogen capping is applied, the equilibrium distance is shortened by about 0.1 Å and its frequency is considerably blue-shifted.

When the NMR chemical shift deviations (shown in Table 3) are examined, a more heterogeneous picture arises. The conventional H- and F-based cappings are only in very rough agreement with the reference system, while both capping potentials yield satisfactory results. When the latter two are compared, it turns out that in our presently optimized capping potential (V_{cap}), the first (C_{11}) and third (C_5) carbon atoms exhibit somewhat larger deviations than the potential from ref 49, while the intermediate carbon (C_8) and most of the hydrogens show better agreement. It is not clear at present what is the specific reason for these deviations in terms of the capping parameters (given numerically in Table 1). It is obvious, however, that the two capping potentials have very different characteristics in terms of the range of their local and nonlocal parts; in particular, the radius of the local part (r_{loc}) differs by a factor of more than 3, as does r_1.

Nevertheless, this result clearly illustrates that the ABC algorithm with its stochastic elements has the very important ability

Table 2. Optimized Bond Lengths, Angles, and Dihedrals of the Octane Reference Molecule and Its Capped Counterpart

	reference	V_{cap}	hydrogen	fluorine	ref 49
C_1-C_5 (Å)	1.54	1.55	1.55	1.54	1.55
C_5-C_8 (Å)	1.55	1.55	1.55	1.55	1.55
C_8-C_{11} (Å)	1.55	1.54	1.55	1.53	1.55
$C_{11}-V_{cap}$ (Å)	1.55	1.62	1.10	1.47	1.55
$C_1-C_5-C_8$ (deg)	113.4	113.5	113.6	113.1	113.7
$C_5-C_8-C_{11}$(deg)	113.6	113.5	113.6	111.7	113.4
$C_8-C_{11}-V_{cap}$ (deg)	114.0	113.7	111.3	110.2	116.2
$C_1-C_5-C_8-C_{11}$ (deg)	−179.3	−179.9	179.8	−179.6	−177.2
$C_5-C_8-C_{11}-V_{cap}$ (deg)	−179.5	−178.2	−179.3	179.6	179.7

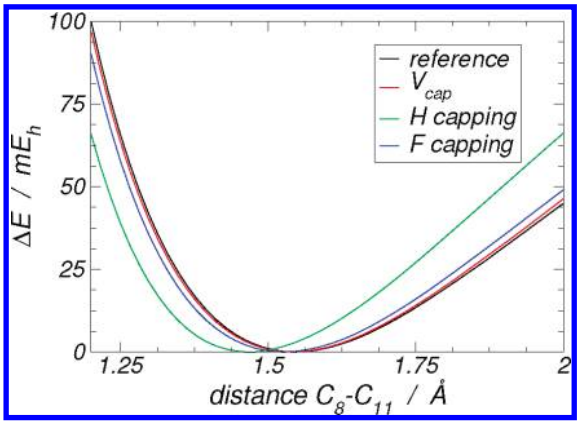

Figure 12. Potential energy curve of the C_8-C_{11} bond.

Table 3. ^{1}H and ^{13}C NMR Chemical Shift Changes of the Capped Octane Molecule with Respect to Its Octane Reference, $\Delta\delta = \sigma^{cap} - \sigma^{ref}$

	chemical shift change (ppm)			
Δδ	V_{cap}	hydrogen	fluorine	ref 49
C_1	0.16	−0.08	0.56	0.56
H_2	0.03	0.01	−0.02	0.02
H_3	0.04	0.01	−0.06	0.03
H_4	0.04	0.02	−0.05	0.02
C_5	−5.03	−1.56	6.77	−1.12
H_6	0.12	0.07	0.14	0.14
H_7	0.13	0.07	0.15	0.22
C_8	−0.02	5.52	0.81	−0.32
H_9	−0.40	−0.07	−0.47	−0.34
H_{10}	−0.41	−0.06	−0.48	−0.41
C_{11}	12.08	18.01	−52.08	−2.44
H_{12}	−0.23	0.37	−3.49	−0.18
H_{13}	−0.24	0.36	−3.47	−0.15

to discover new regions of parameter space, which a downhill algorithm (e.g., conjugate gradients) would never explore. In order to obtain better capping potentials in terms of spectroscopic parameters, the optimization can now be adjusted by means of weighting factors and the exact definition of penalty integration volume. However, this is beyond the scope of the present work and will be highlighted in a forthcoming article.

4. CONCLUSION

In this work, we have presented an algorithmic extension of a numerical optimization scheme for capping potentials that can be used for mixed quantum−classical (QM/MM) ab initio calculations. The new algorithm mixes deterministic (downhill gradient) techniques with stochastic (Monte Carlo-like) moves, which are applied to an analytic potential such that the electronic structure in the quantum region is preserved as well as possible with respect to a reference (full-QM) calculation. Deviations from the ideal electronic (and geometric) structure are characterized by a suitably designed penalty functional, which represents the target quantity that is minimized with respect to the parameters of the capping potential.

Our algorithm is a variant of the artificial bee colony (ABC) approach, which has certain analogies to the foraging behavior of honeybees in nature. From a computational view, it bears similarities to the ideas used in parallel tempering schemes. The stochastic elements that are incorporated into the ABC optimization avoid trapping in local minima of the penalty functional hypersurface. For the benchmark molecule (ethane) used in this work, this surface is still relatively smooth; however, as soon as more complex molecules are targeted, the stochastic components of the ABC algorithm are very important due to the presence of numerous wiggles in this surface. This could be shown by using a randomized starting point for the capping potential optimization. For such more complex situations, several control parameters of the ABC scheme can be adjusted in order to improve the convergence behavior.

The properties of the resulting capping potentials have been characterized in terms of the deviations of carbon NMR chemical shift values with respect to a reference calculation. For our homolytic cleavage of a $C^{sp3}-C^{sp3}$ bond, the properties resemble those of the optimized capping potentials that were obtained previously by the deterministic simplex minimization approach.[49] In turn, our new algorithm has found a considerably different set of values of the capping parameters, mainly because of the use of a slightly different set of weighting parameters within the penalty functional. This illustrates that the penalty surface has indeed a rich substructure, even in a very simple case such as the homolytic capping of ethane.

We believe that the new ABC optimization scheme will help generating better capping potentials for more complex situations in which special care is necessary. In particular, we are presently applying the algorithm to heterolytic bond cleavage (i.e., C−N and C−O bonds), as well as the capping of highly polar and charged groups (i.e., COOH and COO^-), which are of crucial importance for most biophysical QM/MM simulations.

■ ASSOCIATED CONTENT

Supporting Information. Additional text and one figure describing complementary benchmark optimization. This material is available free of charge via the Internet at http://pubs.acs.org.

■ AUTHOR INFORMATION

Corresponding Author
*E-mail: daniel.sebastiani@fu-berlin.de.

■ ACKNOWLEDGMENT

This work has been supported by the German Research Foundation (DFG) under Grants SE 1008/5 and SE 1008/6. Computing infrastructure was provided by the Northern German Supercomputing Alliance (HLRN) under Grant HLRN/bec00061.

■ REFERENCES

(1) Gascon, J. A.; Sproviero, E. M.; Batista, V. S. *J. Chem. Theory Comput.* **2005**, *1*, 674–685.
(2) Kongsted, J.; Nielsen, C. B.; Mikkelsen, K. V.; Christiansen, O.; Ruud, K. *J. Chem. Phys.* **2007**, *126*, No. 034510.
(3) Sebastiani, D. *Nachr. Chem.* **2009**, *57*, 305.
(4) Schmidt, J.; Hoffmann, A.; Spiess, H. W.; Sebastiani, D. *J. Phys. Chem. B* **2006**, *110*, 23204–23210.
(5) Schmidt, J.; Hutter, J.; Spiess, H. W.; Sebastiani, D. *ChemPhysChem* **2008**, *9*, 2313–2316.
(6) Heller, J.; Elgabarty, H.; Zhuang, B.; Sebastiani, D.; Hinderberger, D. *J. Phys. Chem. B* **2010**, *114*, 7429–7438.
(7) Banyai, D. R.; Murakhtina, T.; Sebastiani, D. *Magn. Reson. Chem.* **2010**, *48*, S56–S60.
(8) Ludueña, G. A.; Wegner, M.; Bjâlie, L.; Sebastiani, D. *ChemPhysChem* **2010**, *11*, 2353–2360.
(9) Hansen, M. R.; Sekharan, S.; Graf, R.; Sebastiani, D. *J. Am. Chem. Soc.* **2009**, 5251–5256.
(10) Gervais, C.; Dupree, R.; Pike, K. J.; Bonhomme, C.; Profeta, M.; Pickard, C. J.; Mauri, F. *J. Phys. Chem. A* **2005**, *109*, 6960–6969.
(11) Yates, J. R.; Dobbins, S. E.; Pickard, C. J.; Mauri, F.; Ghi, P. Y.; Harris, R. K. *Phys. Chem. Chem. Phys.* **2005**, *7*, 1402–1407.
(12) Yates, J. R.; Pham, T. N.; Pickard, C. J.; Mauri, F.; Amado, A. M.; Gil, A. M.; Brown, S. P. *J. Am. Chem. Soc.* **2005**, *127*, 10216–10220.
(13) Murakhtina, T.; Delle Site, L.; Sebastiani, D. *ChemPhysChem* **2006**, *7*, 1215–1219.
(14) Rohrig, U.; Guidoni, L.; Laio, A.; Frank, I.; Rothlisberger, U. *J. Am. Chem. Soc.* **2004**, *126*, 15328–15329.
(15) Deng, R. Z.; Martyna, G. J.; Klein, M. L. *Phys. Rev. Lett.* **1993**, *71*, 267.
(16) Stanton, R. V.; Little, L. R.; Merz, K. M. *J. Phys. Chem.* **1996**, *99*, 11266.
(17) Eichinger, M.; Tavan, P.; Hutter, J.; Parrinello, M. *J. Chem. Phys.* **1999**, *21*, 10452.
(18) Lyne, P.; Hodosceck, M.; Karplus, M. *J. Phys. Chem. A* **1999**, *103*, 3462–3471.
(19) Field, M. J.; Bash, P. A.; Karplus, M. *J. Comput. Chem.* **1990**, *11*, 700–733.
(20) Zhang, Y.; Lee, T.-S.; Yang, W. *J. Phys. Chem.* **1999**, *110*, 46–54.
(21) Brancato, G.; Rega, N.; Barone, V. *J. Chem. Phys.* **2008**, *128*, 144501.
(22) Cui, Q. *J. Chem. Phys.* **2002**, *117*, 4720–4728.
(23) Laio, A.; VandeVondele, J.; Roethlisberger, U. *J. Chem. Phys.* **2002**, *116*, 6941–6947.
(24) Cui, Q.; Karplus, M. *J. Chem. Phys.* **2000**, *112*, 1133.
(25) Laio, A.; VandeVondele, J.; Rothlisberger, U. *J. Phys. Chem. B* **2002**, *106*, 7300–7307.
(26) Bühl, M.; Grigoleit, S.; Kabrede, H.; Mauschick, F. T. *Chem.—Eur. J.* **2006**, *12*, 477–488.
(27) Senn, H. M.; Thiel, W. *Top. Curr. Chem.* **2007**, *268*, 173–290.
(28) Kastner, J.; Thiel, S.; Senn, H. M.; Sherwood, P.; Thiel, W. *J. Chem. Theory Comput.* **2007**, *3*, 1064–1072.

(29) Geerke, D. P.; Thiel, S.; Thiel, W.; van Gunsteren, W. F. *Phys. Chem. Chem. Phys.* **2008**, *10*, 297–302.
(30) Benighaus, T.; Thiel, W. *J. Chem. Theory Comput.* **2008**, *4*, 1600–1609.
(31) Komin, S.; Gossens, C.; Tavernelli, I.; Röthlisberger, U.; Sebastiani, D. *J. Phys. Chem. B* **2007**, *111*, 5225–5232.
(32) Singh, U. C.; Kollman, P. A. *J. Comput. Chem.* **1986**, *7*, 718.
(33) Birge, R. R.; Zhang, C.-F. *J. Chem. Phys.* **1990**, *92*, 7178–7195.
(34) Assfeld, X.; Rivail, J.-L. *Chem. Phys. Lett.* **1996**, *263*, 100–106.
(35) Jacob, C. R.; Visscher, L. *J. Chem. Phys.* **2006**, *125*, No. 194104.
(36) Gao, J.; Amara, P.; Alhambra, C.; Field, M. J. *J. Phys. Chem. A* **1998**, *102*, 4714–4721.
(37) Pu, J.; Gao, J.; Truhlar, D. G. *J. Phys. Chem. A* **2004**, *108*, 632–650.
(38) Jung, J.; Choi, C. H.; Sugita, Y.; Ten-no, S. *J. Chem. Phys.* **2007**, *127*, No. 204102.
(39) Jardilliera, N.; Goursot, A. *Chem. Phys. Lett.* **2008**, *454*, 65–69.
(40) Mallik, A.; Taylor, D. E.; Runge, K.; Dufty, J. W. *Int. J. Quantum Chem.* **2004**, *100*, 1019–1025.
(41) DiLabio, G. A.; Wolkow, R. A.; Johnson, E. R. *J. Chem. Phys.* **2005**, *122*, No. 044708.
(42) DiLabio, G. A.; Hurley, M. M.; Christiansen, P. A. *J. Chem. Phys.* **2002**, *116*, 9578–9584.
(43) Xiao, C. Y.; Zhang, Y. K. *J. Chem. Phys.* **2007**, *127*, No. 124102.
(44) Poteau, R.; Ortega, I.; Alary, F.; Solis, A. R.; Barthelat, J.-C.; Daudey, J.-P. *J. Phys. Chem. A* **2001**, *105*, 198–205.
(45) Poteau, R.; Alary, F.; Makarim, H. A. E.; Heully, J.-L.; Barthelat, J.-C.; Daudey, J.-P. *J. Phys. Chem. A* **2001**, *105*, 206–214.
(46) Exner, T. E.; Mezey, P. G. *J. Comput. Chem.* **2003**, *24*, 1980–1986.
(47) Exner, T. E.; Mezey, P. G. *Phys. Chem. Chem. Phys.* **2005**, *24*, 4061–4069.
(48) Eckard, S.; Exner, T. E. *Z. Phys. Chem.* **2006**, *220*, 927–944.
(49) Komin, S.; Sebastiani, D. *J. Chem. Theory Comput.* **2009**, *5*, 1490–1498.
(50) Goedecker, S.; Teter, M.; Hutter, J. *Phys. Rev. B* **1996**, *54*, 1703.
(51) Hartwigsen, C.; Goedecker, S.; Hutter, J. *Phys. Rev. B* **1998**, *58*, 3641.
(52) Rohrig, U. F.; Sebastiani, D. *J. Phys. Chem. B* **2008**, *112*, 1267–1274.
(53) Debye, P. *Math. Ann.* **1909**, *67*, 535–558.
(54) Hestenes, M. R.; Stiefel, E. *J. Res. Natl. Bur. Stand. (U.S.)* **1952**, *49*, 409–436.
(55) Nelder, J. A.; Mead, R. *Comput. J.* **1965**, *7*, 308–313.
(56) Holland, J. H. *Adaptation in natural and artificial systems*; University of Michigan: Ann Arbor, MI, 1975.
(57) Wang, Q. H. *Biol. Cybern.* **1987**, *57*, 95–101.
(58) Yang, X. S. *Lect. Notes Comput. Sci.* **2005**, *3562*, 317–323.
(59) Karaboga, D.; Basturk, B. *J. Global Opt.* **2007**, *39*, 459–471.
(60) Karaboga, D.; Basturk, B. *Appl. Soft Comput.* **2008**, *8*, 687–697.
(61) Karaboga, D.; Akay, B. *Artif. Intell. Rev.* **2009**, *31*, 61–85.
(62) Brown, S. P.; Spiess, H. W. *Chem. Rev.* **2001**, *101*, 4125.
(63) Spiess, H. W. *Macromol. Chem. Phys.* **2003**, *204*, 340–346.
(64) Schulz-Dobrick, M.; Metzroth, T.; Spiess, H. W.; Gauss, J.; Schnell, I. *ChemPhysChem* **2005**, *6*, 315–327.
(65) Ochsenfeld, C.; Brown, S. P.; Schnell, I.; Gauss, J.; Spiess, H. W. *J. Am. Chem. Soc.* **2001**, *123*, 2597–2606.
(66) Bühl, M.; Kabrede, H.; Diss, R.; Wipff, G. *J. Am. Chem. Soc.* **2006**, *128*, 6357–6368.
(67) von Lilienfeld-Toal, A.; Tavernelli, I.; Rothlisberger, U.; Sebastiani, D. *J. Chem. Phys.* **2005**, *122*, No. 014113.
(68) Hohenberg, P.; Kohn, W. *Phys. Rev.* **1964**, *136*, B864.
(69) Kohn, W.; Sham, L. J. *Phys. Rev.* **1965**, *140*, A1133.
(70) Jones, R. O.; Gunnarsson, O. *Rev. Mod. Phys.* **1989**, *61*, 689–746.
(71) Becke, A. D. *Phys. Rev. A* **1988**, *38*, 3098.
(72) Lee, C.; Yang, W.; Parr, R. G. *Phys. Rev. B* **1988**, *37*, 785–789.
(73) Hutter, J.; Curioni, A. *ChemPhysChem* **2005**, *6*, 1788–1793.
(74) Hutter, J. et al. Computer code CPMD, version 3.12.0, Copyright IBM Corp. and MPI-FKF Stuttgart 1990—2007, http://www.cpmd.org.
(75) Putrino, A.; Sebastiani, D.; Parrinello, M. *J. Chem. Phys.* **2000**, *113*, 7102–7109.
(76) Sebastiani, D.; Parrinello, M. *J. Phys. Chem. A* **2001**, *105*, 1951.
(77) Sebastiani, D.; Goward, G.; Schnell, I.; Spiess, H. W. *J. Mol. Struct. (THEOCHEM)* **2003**, *625*, 283–288.